Check for updates

ENVIRONMENTAL STUDIES

Seasonal bromate formation in the Arctic snowpack: Implications for the bromine biogeochemical cycle

Stefano Frassati[1,2]*, Elena Barbaro[1,2]*, Giulio Cozzi[1,2], Clara Turetta[1,2], Federico Scoto[1,2], Claudia Rossetti[1,2], Marco Roman[1], Matteo Feltracco[1], Kitae Kim[3], François Burgay[4], Alfonso Saiz-Lopez[5], Joseph S. Francisco[6], Ward Van Pelt[7], Feiyue Wang[8], David Cappelletti[2,9], Sofia Lerda[9], Giovanni Bistoni[9], Filippo De Angelis[9], Carlo Barbante[1,2], Andrea Gambaro[1], Andrea Spolaor[1,2]*

Copyright © 2026 The Authors, some rights reserved; exclusive licensee American Association for the Advancement of Science. No claim to original U.S. Government Works. Distributed under a Creative Commons Attribution NonCommercial License 4.0 (CC BY-NC).

Bromine exists in multiple chemical forms in the atmosphere, with bromide (Br^-) being the predominant species in snow. Here, we detect and track the formation of bromate (BrO_3^-) in Arctic snow and propose a mechanism for its production. Our observations reveal relevant BrO_3^- concentrations, reaching up to 5% of total bromine, during springtime. The evidence for the persistence of BrO_3^- in the snowpack and its production as a function of solar radiation suggests a snow-driven photochemical process, with negligible contributions from direct aerosol deposition, and emphasizes the role of the snowpack as a reactive matrix for photooxidation, providing insights into the bromine cycle in the Arctic. Our findings are supported by quantum chemical calculations, which explore both radical and ionic reaction mechanisms and the matrix effect, thereby supporting the role of snowpack in promoting BrO_3^- formation. The presence of BrO_3^- in snowpack represents a reservoir of nonreactive bromine, with potential implications for understanding halogen chemistry in polar environments.

INTRODUCTION

Bromine in polar regions plays an important role in atmospheric processes that influence tropospheric and stratospheric ozone depletion reactions, as well as atmospheric mercury depletion events, with relevant implications for our understanding of the Earth's radiative budget and energy dynamics (*1*, *2*). The presence of bromine in the snowpack of polar regions is caused by direct emissions and deposition of bromide-containing sea spray aerosols, along with the reemission of gas-phase bromine during springtime from photochemical processes over the sea ice, especially over first-year sea ice (*3*–*5*). In the atmosphere, bromine can be present in several forms, both inorganic (*6*, *7*) (such as Br_2, BrO, HOBr, BrCl, and $BrNO_2$) and organic (such as CH_3Br), but its main form in the snowpack is bromide (Br^-) (*8*).

Although bromine activation over first-year sea ice snow is well documented (*3*–*5*), the activation and release of bromine from terrestrial snowpack into the atmosphere remain uncertain. Discordant observations and hypotheses (*9*, *10*) have led to debate regarding the potential storage of bromine in the snowpack (*11*). The photo-stimulated emission of gaseous bromine (Br_2) from the snow surface into the atmosphere has been observed in Greenland and Alaska (*10*, *12*). However, a specific study of the diurnal remobilization of halogens from the snowpack indicated that there was no substantial variation in bromine levels between day and night, suggesting that there is no emission of brominated species into the atmosphere (*13*).

These discrepancies in experimental data therefore affect the accuracy of models that predict, for example, ozone depletion events. The WRF-Chem model, which does not include a halogen chemistry component, overestimates the amount of ozone compared to observation, especially at Arctic coastal sites in the spring (*14*). In contrast, other models that include halogen reactions tend to underestimate total ozone in the Arctic in the early spring and overestimate the emission of reactive bromine species from snow (*15*, *16*). To minimize these effects, the models assume a pool of nonreactive bromine in the snow (*15*, *17*, *18*). The implementation of halogens in a global model highlights the importance of accounting for halogen chemistry to reproduce springtime surface ozone in polar regions accurately and shows that halogen-induced ozone depletion is exported from the Arctic to mid-latitudes (*19*, *20*).

One of such nonreactive bromine species is bromate (BrO_3^-), the ultimate oxidation product of Br^- through reactions with oxidants such as O_3 or •OH (*21*). Numerous studies have documented the presence of oxidant species in snow, including reactive oxygen species (ROS; e.g., O_3, •OH, •OOH, and H_2O_2), some of which are active participants in bromine explosion reactions (*22*–*24*). ROS in the snowpack could be produced through photochemical reactions involving NO_3^- and NO_2^- (at $\lambda_{max} = 320$ nm). These reactions, under acidic conditions (pH < 6), can produce O^-, which rapidly reacts with water to form the •OH (*25*). Alternatively, nitrate photolysis can release atomic oxygen, which may react with dissolved molecular oxygen to form O_3 (*22*, *26*, *27*). At these same wavelengths, H_2O_2 can undergo homolytic photolysis, producing hydroxyl radicals (•OH) (*28*, *29*). Most of these oxidants require ultraviolet (UV) light to be formed in situ in the snowpack. Conversely, ozone can diffuse into the snow from the atmosphere, there being the most effective oxidant in dark conditions. BrO_3^- formation has been well studied in aqueous media, especially in water treatment systems due to its carcinogenic

[1]Department of Environmental Sciences, Informatics and Statistics, Ca' Foscari University of Venice, Venice Mestre, Italy. [2]Institute of Polar Sciences–National Research Council of Italy (CNR-ISP), Venice Mestre, Italy. [3]Korea Polar Research Institute (KOPRI), Incheon 21990, Republic of Korea. [4]Department of Environmental Sciences, University of Basel, 4001 Basel, Switzerland. [5]Department of Atmospheric Chemistry and Climate, Institute of Physical Chemistry Blas Cabrera, CSIC, 28006 Madrid, Spain. [6]Department of Earth and Environmental Science and Department of Chemistry, University of Pennsylvania, Philadelphia, PA 19104, USA. [7]Department of Earth Sciences, Uppsala University, Uppsala, Sweden. [8]Centre for Earth Observation Science, and Department of Environment and Geography, University of Manitoba, Winnipeg, Manitoba, Canada. [9]Department of Chemistry, Biology and Biotechnology, University of Perugia, Perugia, 06123, Italy.
*Corresponding author. Email: stefano.frassati@unive.it (S.F.); elena.barbaro@cnr.it (E.B.); andrea.spolaor@cnr.it (A.S.)

Downloaded from https://www.science.org at Uppsala University on May 06, 2026

properties (*30*, *31*). The initial reaction step for its formation involves the oxidation of bromide to either a bromine atom or hypobromous acid, HOBr. Both pathways could then lead to further oxidation steps to BrO_3^-. However, to the best of our knowledge, no studies have investigated the presence of BrO_3^- in snow.

This study presents the evidence of BrO_3^- in Arctic snowpacks. We experimentally demonstrate that the surface layers of the polar snowpack can create an ideal environment for fostering the oxidation of bromide to BrO_3^- when exposed to sunlight, thereby acting as a nonreactive bromine reservoir that has not yet been considered in current models. We also provide a theoretical framework to understand the oxidation pathways in BrO_3^- formation.

RESULTS

Bromate occurrence in the surface snow and seasonal snowpack

To examine the presence of BrO_3^- in Arctic snowpacks and the mechanism that controls its formation, we designed and conducted specific experiments in the Svalbard archipelago at different sites and with different temporal resolutions. First, to quantify the presence of BrO_3^- in surface snow and evaluate potential in situ production processes, daily snow samples were collected at the Gruvebadet Snow Research Site (GSRS) in Svalbard following a snowfall event, from 28 April to 3 May 2023 (see Materials and Methods). The results revealed a 10-fold increase in BrO_3^- concentration over the 5 days, rising from 0.4 nM on the first day to 4.3 nM on the last day (see fig. S5). Concurrently, bromide (Br^-) concentration increased from 20 to 63 nM, showing a similar trend to BrO_3^- (fig. S5). To determine whether the increase in BrO_3^- was solely related to a parallel rise in bromide, BrO_3^- concentrations were normalized to Br^- concentrations. During the study period, the BrO_3^-/Br^- ratio increased from 2.05×10^{-2} (28 April) to 7.00×10^{-2} (3 May), as shown in Fig. 1.

The second experiment was aimed at investigating the effect of varying solar radiation on the potential bromate production within the seasonal snowpack. We analyzed a series of snow pit samples collected at the GSRS through weekly sampling during the 2021–2022 snow season. Three sets of snowpit samples were collected during the polar night, three during the day/night cycle period and three during the polar day, thus with a full exposure of the upper part of the snowpack to sunlight. BrO_3^- concentrations in the snowpack collected during the polar night and in the day-night cycle period were similar, ranging between 2.0×10^{-2} to 3.6×10^{-1} nM, with a mean value of the BrO_3^-/Br^- ratio of $1.4 \times 10^{-3} \pm 6.6 \times 10^{-4}$. The most superficial samples collected in April 2022 showed higher values of the BrO_3^-/Br^- ratio, up to 2.2×10^{-2} (4.3 nM BrO_3^-), while the deepest samples present BrO_3^- concentrations below the instrumental limit of detection (7.8×10^{-3} nM; fig. S6), due to rain on snow event on 13 March 2022 (Fig. 2). Regarding Br^-, as illustrated in fig. S6, no trend is evident within the snowpack, with an average concentration of 160 ± 104 nM.

Last, snow samples from two snow pits, dug in April and in the accumulation area of two glaciers nearby Ny-Ålesund, Holtedahlfonna (HDF) and Kongsvegen (KNG), were analyzed to evaluate the seasonality in bromate production and concentration in the absence of winter melting and percolation events. The results obtained from the 2022 HDF snow pit (Fig. 3) indicate that the BrO_3^-/Br^- ratio in the lower snow layers is approximately 10 times lower than in the upper layers, ranging from 3.3×10^{-3} (bottom) to 4.9×10^{-2} observed at the top of the snowpack. Similarly, the 2015 KNG snow pit samples show the highest BrO_3^-/Br^- ratio near the surface, reaching a maximum of 3.21×10^{-3} at a depth of 40 cm. In the middle section of the annual snowpack (90 to 140 cm), the ratio decreases to an average value about four times lower than that in the surface layers, before rising again in the deepest part (140 to 200 cm), where it reaches values comparable to those at the top (see Fig. 3 and Materials and Methods for the site description). At both sites, Br^- has an average concentration of 106 ± 60 nM for HDF and 48 ± 41 nM for KNG. As illustrated in fig. S7, in both snow pits, the BrO_3^- appears to increase at the surface, rising from values of ~$5.1 \times 10^{-1} \pm 0.2 \times 10^{-1}$ nM in the deeper samples to a maximum of 2.3 ± 0.5 nM near the surface for HDF. In contrast, for KNG, the lowest layers show values of $9.5 \times 10^{-2} \pm 4.3 \times 10^{-2}$ nM, while the maximum value of 3.8×10^{-1} is found in the layer at a depth of 30 cm.

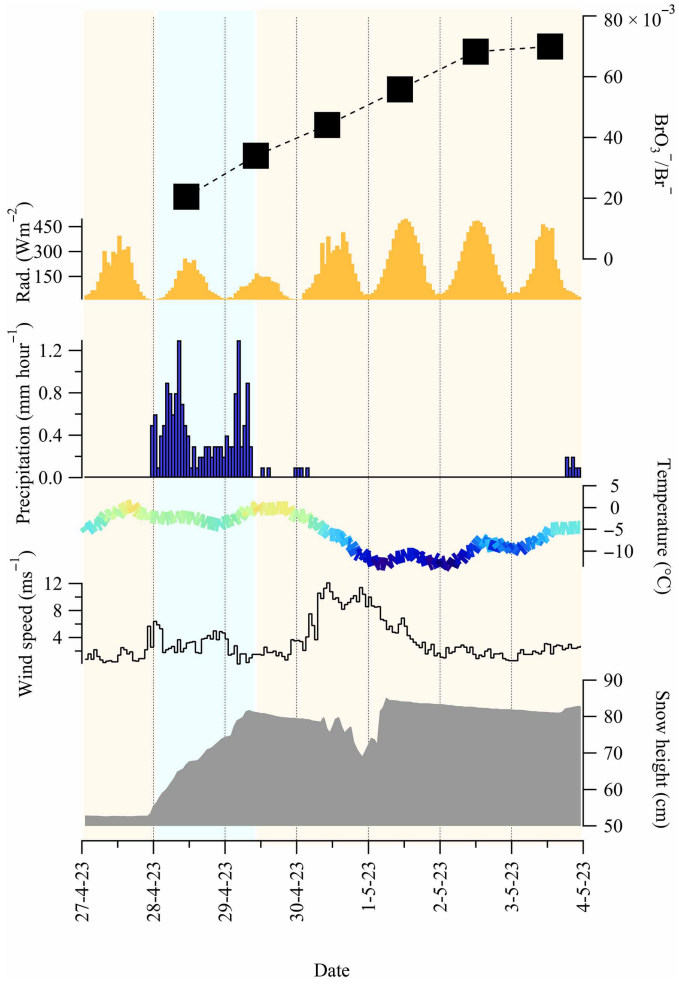

Fig. 1. Daily evolution of BrO_3^-/Br^- ratio levels in surface snow. Trends in BrO_3^- values in relation to meteorological parameters (such as shortwave radiation, precipitation, temperature, and wind speed) and snow height during the period from 28 April to 3 May 2023 at GSRS. Blue band represents the period of precipitation. The meteorological precipitation and snow depth data are shown at hourly frequency (https://seklima.met.no/observations), while the irradiance data are shown at 30-min resolution and come from CCT (*45*). Temperature is represented using a color gradient from blue (colder) to yellow (warmer) to facilitate visual interpretation.

Downloaded from https://www.science.org at Uppsala University on May 06, 2026

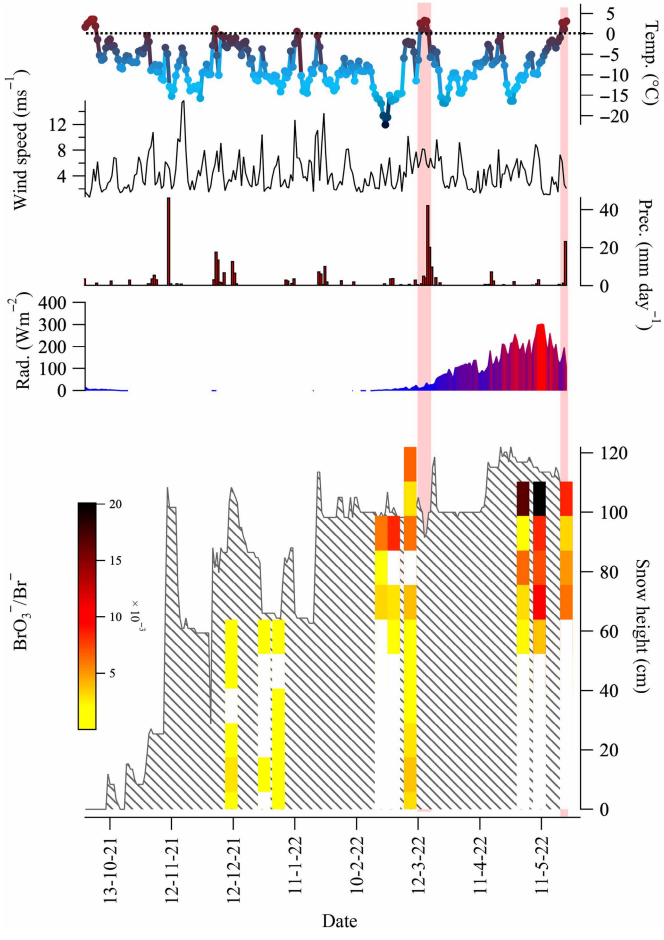

Fig. 2. Seasonal evolution of BrO_3^-/Br^- ratio levels in snow. Time series of bromate in the seasonal snowpack at GSRS in relation to temperature, wind speed, precipitation, and radiation. Samples were collected during the polar night, dawn, and full day. The discrepancy between the height measured during the sampling and the height measured by the automatic measuring device is due to the punctual instrumental measurement, while the sampling area covers an area of 6 m by 10 m with possible surface irregularities and different accumulations of snow. The red band represents the rainfall period. Temperature is represented using a color gradient from blue (colder) to yellow (warmer), and shortwave radiation is shown from blue (lower) to red (higher), to facilitate visual interpretation.

DISCUSSION

The relationship between bromate production and sunlight

The ultimate source of bromine in the snowpack is sea salt aerosols originating from the oceans. Possible mechanisms for BrO_3^- formation in the snowpack include (i) gas-phase reactions during the atmospheric transport of sea salt bromide followed by deposition and (ii) in situ production through oxidation reactions of bromine species in the snowpack.

The first hypothesis is challenged by analyses of aerosol samples collected in Ny-Ålesund from February 2022 to June 2022 (see table S2), which found no traces of BrO_3^- despite showing a trend of methanesulphonic acid (MSA) consistent with prior work in the same area and a Br^- concentration ranging from 1.39 to 20.8 ng m^{-3}. The absence of BrO_3^- in aerosol samples, despite the presence of Br^-, suggests that its formation likely occurs after deposition, within the snowpack itself. In our preliminary data analysis, we observed a correlation between BrO_3^- and MSA concentrations (Pearson's $r = 0.81$, $P < 0.001$; see table S4) in the snowpack, indicating a relationship between the two species. It is well known that the formation of MSA occurs through atmospheric photo-oxidative reactions of dimethylsulfide, a compound released during algal blooms in the atmosphere. Therefore, our first hypothesis is that BrO_3^- may originate from photochemical processes in the atmosphere after being released as bromide from the same marine source as MSA. A second possibility is that the production processes for MSA and BrO_3^- are both linked to solar radiation but in different contexts (i.e., atmosphere versus snowpack), leading to only an apparent correlation between their final concentrations. The connection with photochemistry has been documented for MSA in the atmosphere, but not for bromate in snow.

Considering the daily sampling of surface snow in Ny-Ålesund (Fig. 1), the observed increase, during sunrise, of the BrO_3^-/Br^- ratio began after a 2-day snowfall followed by a regular sunlight illumination cycle, with bromate concentrations continuously increasing and peaking after ~5 days. The radiation data (Fig. 1B) were collected at the Amundsen-Nobile climate change tower (CCT), located 500 m from the snow sampling site. Radiation reaching the surface is typically extinguished within the first 10 cm of snow (*23*). For samples that were never exposed to sunlight, the BrO_3^-/Br^- ratio values remained low and relatively constant. However, during sunrise, the BrO_3^-/Br^- ratio values in the sunlight-exposed layers gradually increased, suggesting an effective mechanism for BrO_3 production triggered by sunlight (Fig. 2). The formation of the snowpack in the HDF experiment was characterized by a few but intense snowfalls (~15 cm), allowing prolonged exposure of the surface layer to solar radiation (Fig. 3A). In contrast, the KNG snowpack experienced several less intense snowfalls (<10 cm) that reduced the exposure time of the surface snow layer to sunlight (Fig. 3B). Consistently, we observed the lowest BrO_3^- values in the deepest dark snow layers, whereas the illuminated surface layers showed an increase in concentration.

The results indicate at least two mechanisms for BrO_3^- formation. The first, related to sunlight intensity, involves the photochemical production of radicals in the snowpack. Specifically, the reaction between BrO and $BrONO_2$ generates HOBr in solution, which, under UV irradiation, produces Br radicals, subsequently oxidized by the OH radical (Fig. 4A, top) (*21*). A second mechanism, also active in the dark, may follow an ionic pathway mediated by O_3 and/or the OH radical, similar to that observed for Cl^- in Arctic and Antarctic snow samples (*32*–*34*), as shown in Fig. 4A (bottom) and in the Supplementary Materials. This pathway is well known in wastewater treatment. In this case, starting from Br^-, a series of oxidative steps leads to the formation of BrO_3^-. Laboratory studies have investigated BrO_3^-reduction reactions in ice by stimulating specific processes. Since these experiments are conducted in controlled environments, it is plausible that BrO_3^-reduction in natural snow is negligible. Both computational and experimental studies support the idea that the oxidation reaction of Br^- can occur at the gas-liquid interface (*35*–*38*). It is reasonable to hypothesize that bromate production might happen within the concentrated brine regions that form during freezing. These brines consist of highly concentrated aqueous solutions located between ice grains or at the ice-air interface. It has been demonstrated that within such brines, dissolved species can undergo a substantial increase in concentration, with some studies reporting up to a 10,000-fold enhancement (*24*, *39*).

Downloaded from https://www.science.org at Uppsala University on May 06, 2026

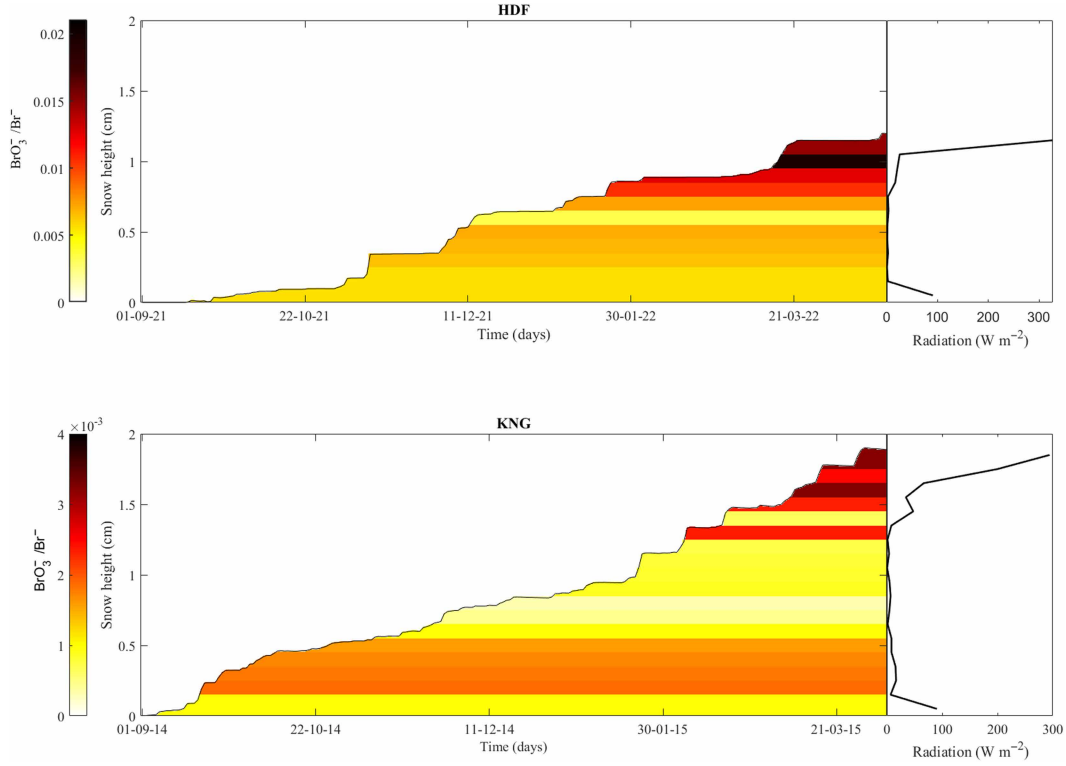

Fig. 3. Cumulative BrO_3^-/Br^- ratio production in glacier snow. Trend of BrO_3^-/Br^- ratio measurements in seasonal snow samples in the HDF (top, sampled in 2022) and KNG (bottom, sampled in 2015) glaciers. The graphs on the right show the radiation penetrated across 10-cm depth (refer to Materials and Methods), using the incoming radiation data from the CCT. Regarding HDF, sampling took place on 24 April 2022, while regarding KNG, it took place on 10 April 2015.

To shed light on these hypotheses, we conducted a quantum mechanical calculation (see the Supplementary Materials for details) to ensure a consistent understanding of the proposed reaction mechanisms. The photodissociation of HOBr triggers the first mechanism (Fig. 4B, left) and proceeds through radical intermediates. The second mechanism (Fig, 4B, right) involves only ionic species and begins with the oxidation of Br^- by ozone. Both mechanisms involve multiple spin transitions, necessitating the calculation of sections of potential energy surfaces with different spin multiplicities. In addition, calculations were performed both in the gas phase and in the presence of water using the implicit solvent model C-PCM (Water).

The potential energy surface of the proposed radical mechanism initiated by photo-absorption is shown in Fig. 4 (left-hand side), which reports the relative free energies of all intermediates computed in the gas phase (red) and in water (black). The photodissociation of HOBr requires an initial energy of 43.7 kcal/mol. Notably, while all the successive steps involving the oxidation of Br are considerably exergonic and irreversible in water, the situation changes markedly in the gas phase. In particular, when simulated in the gas phase rather than in water, one step (the third) even switches from exergonic to endergonic.

The right-hand of Fig. 4 displays the computed section of the potential energy surface for the alternative ionic mechanism. The steps of this mechanism were found to be exergonic in both the presence and absence of the solvent. The first step of the ionic mechanism presents an energy barrier which was further examined by (i) calculating the transition states for both the singlet and triplet states and (ii) identifying the minimum energy crossing point between their potential energy surfaces. Two possible pathways were found. In the "early" crossing scenario (fig. S12), the singlet-triplet crossing occurs before the transition state, while in the "late" crossing case (fig. S13), it occurs afterward. The latter corresponds to the minimum energy path, with an associated energy barrier of 20.7 kcal/mol.

The existence of notable reaction barriers at the entrance of both radical and ionic channels is a possible explanation for the generally low efficiency of bromate formation in the snowpack. However, the initial reaction barrier associated with the photodissociation of HOBr in the radical mechanism can be overcome by the action of sunlight. On the other hand, the ionic mechanism may operate even in the dark but with low efficiency due to the energy barrier associated with crossing singlet-triplet potential energy surfaces.

The calculations suggest that the radical mechanism should occur in the brine layer, while the ionic mechanism could also be effective in the interstitial air of the snowpack. Reactive species such as OH radicals can be formed from the photolysis of NO_3^-. Nevertheless, the correlations shown in table S3 do not demonstrate a direct link between BrO_3^- production and NO_3^-. This may be due to the consumption of reactive species by other compounds, leading to an absence of a direct correlation with NO_3^-, which could produce, in large excess, the reactive species useful for the oxidation of Br^-. Furthermore, the observed correlation value between BrO_3^- and Br^- indicates that bromide is present in excess of the reactive species. This suggests that it should not be considered a limiting reagent and that UV radiation is the primary driver for BrO_3^- formation.

Downloaded from https://www.science.org at Uppsala University on May 06, 2026

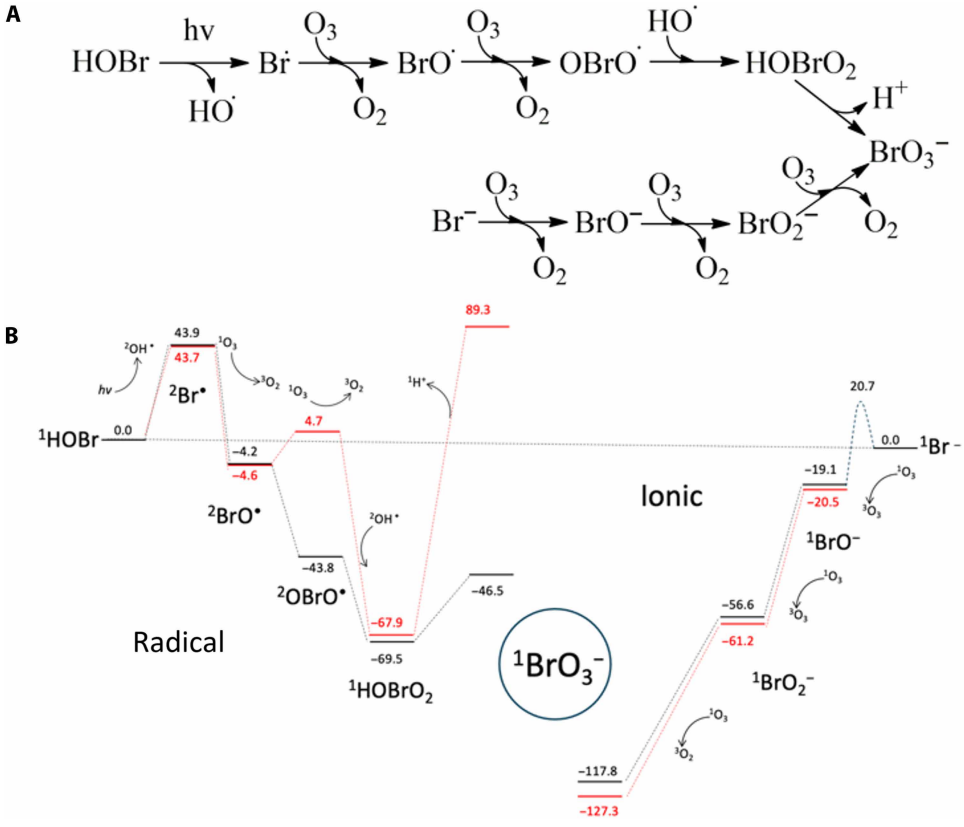

Fig. 4. Reaction pathways and potential energy surfaces for the oxidation of Br^- to BrO_3^- via radical and ionic mechanisms. (**A**) Reaction pathway and (**B**) potential energy surface of the radical and ionic mechanisms computed at WB97X-D3BJ level of theory. Gas-phase results are reported in red, while calculations performed with the implicit solvent model C-PCM(Water) are reported in black.

Implication of bromate formation in snowpack

Our study shows that bromate forms in the Arctic snowpack because sunlight causes bromide oxidation, trapping an important portion of bromine (up to 5%) and reducing the pool of reactive bromine. Although this percentage may seem small, it is particularly relevant from a modeling perspective. Bromate is the most stable form of bromine, meaning that this amount can stay locked in seasonal snow cover, lessening bromine available for bromine explosions. This process, which had not been considered before, could enhance current atmospheric and geochemical models of the bromine cycle.

The snowpack, particularly under solar irradiation, emerges as a highly oxidizing environment, emphasizing the need for further studies on its role in polar region chemistry. Future experimental and theoretical investigations are necessary to refine the kinetic parameters governing bromate formation and stability in snow. The inclusion of a nonreactive bromine pool is a key element in improving the implementation of predictive models of the ozone depletion process, helping to reduce prediction errors, particularly during periods characterized by a marked day-night cycle.

Furthermore, the accumulation of bromate in Arctic snow during winter implies its potential release into the environment during the melting season, which has implications for biogeochemical cycling. Beyond the Arctic, this mechanism may also apply to other snow-covered regions, including Antarctica and mid-latitude mountain ranges like the Alps. Understanding bromate formation in these environments could offer broader insights into the role of snowpack photochemistry in atmospheric halogen cycles and its effects on climate-related processes

MATERIALS AND METHODS

Snow pit sampling

Nearby GSRS [78.55°N, 11.53°E; 50 m above sea level (a.s.l.); fig. S1], a weekly snow pit sampling was done to collect snow samples and physical parameters such as temperature and density. Daily surface snow samples were collected between 28th April and 3rd May 2023 at 12 midday. For the seasonal study, three series of samples taken during the polar night and another three series during the all-day period were used.

Snow samples from glaciers were collected from a snow pit near stake 3 (78.95°N, 13.40°E, 600 m a.s.l.) on the HDF ice cap on 24 April 2022. HDF is the largest ice cap (~300 km^2) on north-western Spitsbergen, about 40 km from the Ny-Ålesund station. It is distributed over an elevation range of 0 to 1241 m a.s.l. The front of KNG is located ~20 km to the east of Ny-Alesund extending about 20 km inland. Samples were collected at stake 8 (78.45°N, 13.20°E, 750 m a.s.l.) on 10 April 2015 (see the Supplementary Materials). No permits or authorizations were required for the collection of the samples used.

After excavation, ~10 cm of snow was removed from the pit wall to create a clean sampling surface and avoid contamination introduced during excavation. The snow wall was sampled using polyethylene

Downloaded from https://www.science.org at Uppsala University on May 06, 2026

precleaned tubes with a depth interval of 10 cm so that 12 samples were taken for each snow pit. Snow pit samples were transported frozen (−20°C) and in dark conditions directly to the Institute of Polar Sciences–National Research Council (ISP-CNR) laboratories in Venice, where they were melted at room temperature under a laminar flow bench (class 100) inside a clean room.

Aerosol sampling

Aerosol samples were collected using a PM10 high-volume air sampler (TE-6070) operating at a flow rate of 68 m^3 $hour^{-1}$. The sampler was fitted with an 8″ × 10″ quartz fiber filter that had been precombusted for 4 hours at 400°C in a muffle furnace. Field blanks were obtained by placing the same filters on the sampler with the air pump turned off. Both samples and blanks were stored and transported at −20°C in dark conditions. Bromate was extracted by sonication (30 min) in ultrapure water (10 ml) (*40*).

Analytical measurements

Snow speciation analyses were carried out by an ion chromatography system (Dionex-2100, Thermo Fisher Scientific) coupled with inductively coupled plasma sector field mass spectrometer (Element XR, Thermo Fisher Scientific). The chromatographic separation was performed on a Dionex Ion AS19 anion exchange column (2 mm by 250 mm) with a Dionex IonPac AG19 guard column (2 mm by 50 mm). The instrumental detection (LOD) calculated were 5×10^{-2} nM for Br^- and 8×10^{-3} nM for BrO_3^-, respectively (*41*).

Quantification of BrO_3^- in the aerosol samples was performed with an Anion Exchange Chromatography-Pulsed Amperometric Detection (HPAEC, Dionex, Thermo Fisher Scientific, ICS-5000, Waltham, USA) coupled to a TSQ Altis Plus triple quadrupole mass spectrometer (Thermo Fisher Scientific, ICS-5000, Waltham, USA) using a heated electrospray source operating in negative mode. Chromatographic separation, carried out with a KOH gradient, was performed using a Dionex IonPac AS24 RFIC 2 mm–by–250 mm anion-exchange column (Thermo Fisher Scientific) equipped with a Dionex IonPac AG24 RFIC 2 mm–by–50 mm guard column (Thermo Fisher Scientific) (*40*).

Major anions were determined using an ion chromatography system (Thermo Fisher Scientific, Dionex ICS-5000, Waltham, MA, USA), coupled to a single quadrupole mass spectrometer (MSQ Plus, Thermo Fisher Scientific, Bremen, Germany), while cations were determined using the same ion chromatograph coupled to a conductivity detector, following a previously published method (*42*). A multianion standard for ion chromatography [Cl^- (10 mg $liter^{-1}$), NO_3^- (20 mg $liter^{-1}$), Br^- (20 mg $liter^{-1}$), and SO_4^{2-} (20 mg $liter^{-1}$)] and single standard solution of MSA (1000 mg $liter^{-1}$) were purchased from Sigma-Aldrich. The multication standard solution for ion chromatography (Ca^{2+}, Na^+, and NH_4^+) at the concentration of 100 mg $liter^{-1}$ was provided by Sigma-Aldrich (*43*). Correlation matrices are available in the Supplementary Materials.

In the case of BrO_3^- values that fell below the LOD, these were not included in the calculation of the BrO_3^-/Br^- ratio. Furthermore, in the color bar of the graphs, these values were represented in gray.

Snowpack modeling and snow pit dating

To reconstruct the evolution of the snowpack during the season, a coupled energy balance–snow modeling system was used (*5*, *6*) It simulates multilayer snow density, temperature, and water content with <5-cm vertical resolution, in response to water transport, storage, and refreezing, as well as gravitational compaction and heat diffusion. The model is based on (*5*) but uses a new description of fresh snow density and snow compaction following (*6*). Here, the model is forced with meteorological data from the Norwegian Hindcast Archive (NORA3) reanalysis dataset (*44*), providing fields at 3-km spatial resolution, which are then downscaled to a 1-km resolution grid as described in (*5*). From the model output, we extract seasonal snow height as a function of time for the period from 1 September (2014 for KNG and 2021 for HDF) to the day of sampling. Model values were then rescaled to the snow depth measured on the day of sampling to remove biases while maintaining temporal variability. It is noteworthy that the NORA3 reanalysis dataset assimilated weather station data, e.g., from the Ny-Ålesund weather station, thereby assuring similar meteorological conditions close to weather station locations. The radiation for each 10-cm layer was calculated by integration of the following formula below, considering the 10-cm photic zone

$$R_d = R_0 \exp\left(\frac{d - d_0}{z_e}\right)$$

where R_d is the radiation at depth d, R_0 is the incident radiation [data acquired at the CCT (*45*)], $d - d_0$ is the depth difference (in this work, assumed 1 cm), and z_e is the e-folding depth, assuming it to be constant (equal to 2 cm^{-1}) considering the photic zone to be 10 cm and assuming the snowpack to be constant in terms of microstructure and density.

Computational details

All calculations were carried out using the ORCA quantum chemistry program package (*46*, *47*). Unless otherwise specified, density functional theory calculations were carried out using the WB97-X exchange correlation functional (*48*). Dispersion corrections were incorporated using the Grimme's D3 correction combined with the Becke-Johnson damping functions (D3BJ) (*49*). The def2-TZVP basis set was used (*50*). Implicit solvation effects in water were accounted for using the C-PCM method (*51*, *52*). Thermal corrections were computed at 298 K.

Supplementary Materials

This PDF file includes:

Supplementary Text
Tables S1 to S6
Figs. S1 to S13
References

REFERENCES

1. W. R. Simpson, R. Von Glasow, K. Riedel, P. Anderson, P. Ariya, J. Bottenheim, J. Burrows, L. J. Carpenter, U. Frieß, M. E. Goodsite, D. Heard, M. Hutterli, H.-W. Jacobi, L. Kaleschke, B. Neff, J. Plane, U. Platt, A. Richter, H. Roscoe, R. Sander, P. Shepson, J. Sodeau, A. Steffen, T. Wagner, E. Wolff, Halogens and their role in polar boundary-layer ozone depletion. *Atmos. Chem. Phys.* **7**, 4375–4418 (2007).
2. A. Saiz-Lopez, R. P. Fernandez, Q. Li, C. A. Cuevas, X. Fu, D. E. Kinnison, S. Tilmes, A. S. Mahajan, J. C. Gómez Martín, F. Iglesias-Suarez, R. Hossaini, J. M. C. Plane, G. Myhre, J.-F. Lamarque, Natural short-lived halogens exert an indirect cooling effect on climate. *Nature* **618**, 967–973 (2023).
3. D. Segato, A. Saiz-Lopez, A. S. Mahajan, F. Wang, J. P. Corella, C. A. Cuevas, T. Erhardt, C. M. Jensen, C. Zeppenfeld, H. A. Kjær, C. Turetta, W. R. L. Cairns, C. Barbante, A. Spolaor, Arctic mercury flux increased through the Last Glacial Termination with a warming climate. *Nat. Geosci.* **16**, 439–445 (2023).
4. K. Abrahamsson, A. Granfors, M. Ahnoff, C. A. Cuevas, A. Saiz-Lopez, Organic bromine compounds produced in sea ice in Antarctic winter. *Nat. Commun.* **9**, 5291 (2018).
5. P. Vallelonga, N. Maffezzoli, A. Saiz-Lopez, F. Scoto, H. A. Kjær, A. Spolaor, Sea-ice reconstructions from bromine and iodine in ice cores. *Quat. Sci. Rev.* **269**, 107133 (2021).

Downloaded from https://www.science.org at Uppsala University on May 06, 2026

6. K. L. Foster, R. A. Plastridge, J. W. Bottenheim, P. B. Shepson, B. J. Finlayson-Pitts, C. W. Spicer, The role of Br_2 and BrCl in surface ozone destruction at polar sunrise. *Science* **291**, 471–474 (2001).
7. X. Yang, J. A. Pyle, R. A. Cox, N. Theys, M. Van Roozendael, Snow-sourced bromine and its implications for polar tropospheric ozone. *Atmos. Chem. Phys.* **10**, 7763–7773 (2010).
8. K. A. Pratt, K. D. Custard, P. B. Shepson, T. A. Douglas, D. Pöhler, S. General, J. Zielcke, W. R. Simpson, U. Platt, D. J. Tanner, L. Gregory Huey, M. Carlsen, B. H. Stirm, Photochemical production of molecular bromine in Arctic surface snowpacks. *Nat. Geosci.* **6**, 351–356 (2013).
9. T. Tang, J. C. McConnell, Autocatalytic release of bromine from Arctic snow pack during polar sunrise. *Geophys. Res. Lett.* **23**, 2633–2636 (1996).
10. K. D. Custard, A. R. W. Raso, P. B. Shepson, R. M. Staebler, K. A. Pratt, Production and release of molecular bromine and chlorine from the arctic coastal snowpack. *ACS Earth Space Chem.* **1**, 142–151 (2017).
11. F. Burgay, R. P. Fernández, D. Segato, C. Turetta, C. S. Blaszczak-Boxe, R. H. Rhodes, C. Scarchilli, V. Ciardini, C. Barbante, A. Saiz-Lopez, A. Spolaor, 200-Year ice core bromine reconstruction at Dome C (Antarctica): Observational and modelling results. *Cryosphere* **17**, 391–405 (2023).
12. J. E. Dibb, L. D. Ziemba, J. Luxford, P. Beckman, Bromide and other ions in the snow, firn air, and atmospheric boundary layer at Summit during GSHOX. *Atmos. Chem. Phys.* **10**, 9931–9942 (2010).
13. A. Spolaor, E. Barbaro, D. Cappelletti, C. Turetta, M. Mazzola, F. Giardi, M. P. Björkman, F. Lucchetta, F. Dallo, K. A. Pfaffhuber, H. Angot, A. Dommergue, M. Maturilli, A. Saiz-Lopez, C. Barbante, W. R. L. Cairns, Diurnal cycle of iodine, bromine, and mercury concentrations in Svalbard surface snow. *Atmos. Chem. Phys.* **19**, 13325–13339 (2019).
14. L. Marelle, J.-C. Raut, K. S. Law, L. K. Berg, J. D. Fast, R. C. Easter, M. Shrivastava, J. L. Thomas, Improvements to the WRF-Chem 3.5.1 model for quasi-hemispheric simulations of aerosols and ozone in the Arctic. *Geosci. Model Dev.* **10**, 3661–3677 (2017).
15. K. Toyota, J. C. McConnell, R. M. Staebler, A. P. Dastoor, Air–snowpack exchange of bromine, ozone and mercury in the springtime Arctic simulated by the 1-D model PHANTAS – Part 1: In-snow bromine activation and its impact on ozone. *Atmos. Chem. Phys.* **14**, 4101–4133 (2014).
16. S. Falk, B.-M. Sinnhuber, Polar boundary layer bromine explosion and ozone depletion events in the chemistry–climate model EMAC v2.52: Implementation and evaluation of AirSnow algorithm. *Geosci. Model Dev.* **11**, 1115–1131 (2018).
17. S. Zhai, W. Swanson, J. R. McConnell, N. Chellman, T. Opel, M. Sigl, H. Meyer, X. Wang, L. Jaeglé, J. Stutz, J. E. Dibb, K. Fujita, B. Alexander, Implications of snowpack reactive bromine production for arctic ice core bromine preservation. *JGR Atmospheres* **128**, e2023JD039257 (2023).
18. W. F. Swanson, C. D. Holmes, W. R. Simpson, K. Confer, L. Marelle, J. L. Thomas, L. Jaeglé, B. Alexander, S. Zhai, Q. Chen, X. Wang, T. Sherwen, Comparison of model and ground observations finds snowpack and blowing snow aerosols both contribute to Arctic tropospheric reactive bromine. *Atmos. Chem. Phys.* **22**, 14467–14488 (2022).
19. R. P. Fernandez, A. Carmona-Balea, C. A. Cuevas, J. A. Barrera, D. E. Kinnison, J. Lamarque, C. Blaszczak-Boxe, K. Kim, W. Choi, T. Hay, A. Blechschmidt, A. Schönhardt, J. P. Burrows, A. Saiz-Lopez, Modeling the sources and chemistry of polar tropospheric halogens (Cl, Br, and I) using the CAM-chem global chemistry-climate model. *J. Adv .Model Earth Syst.* **11**, 2259–2289 (2019).
20. R. P. Fernandez, L. Berná, O. G. Tomazzeli, A. S. Mahajan, Q. Li, D. E. Kinnison, S. Wang, J.-F. Lamarque, S. Tilmes, H. Skov, C. A. Cuevas, A. Saiz-Lopez, Arctic halogens reduce ozone in the northern mid-latitudes. *Proc. Natl. Acad. Sci. U.S.A.* **121**, e2401975121 (2024).
21. C. M. Morrison, S. Hogard, R. Pearce, A. Mohan, A. N. Pisarenko, E. R. V. Dickenson, U. Von Gunten, E. C. Wert, Critical review on bromate formation during ozonation and control options for its minimization. *Environ. Sci. Technol.* **57**, 18393–18409 (2023).
22. H.-W. Jacobi, B. Hilker, A mechanism for the photochemical transformation of nitrate in snow. *J. Photochem. Photobiol. A Chem.* **185**, 371–382 (2007).
23. A. M. Grannas, A. E. Jones, J. Dibb, M. Ammann, C. Anastasio, H. J. Beine, M. Bergin, J. Bottenheim, C. S. Boxe, G. Carver, G. Chen, J. H. Crawford, F. Dominé, M. M. Frey, M. I. Guzmán, D. E. Heard, D. Helmig, M. R. Hoffmann, R. E. Honrath, L. G. Huey, M. Hutterli, H. W. Jacobi, P. Klán, B. Lefer, J. McConnell, J. Plane, R. Sander, J. Savarino, P. B. Shepson, W. R. Simpson, J. R. Sodeau, R. Von Glasow, R. Weller, E. W. Wolff, T. Zhu, An overview of snow photochemistry: Evidence, mechanisms and impacts. *Atmos. Chem. Phys.* **7**, 4329–4373 (2007).
24. J. P. Bower, C. Anastasio, Measuring a 10,000-fold enhancement of singlet molecular oxygen (1O2*) concentration on illuminated ice relative to the corresponding liquid solution. *Atmos. Environ.* **75**, 188–195 (2013).
25. L. Chu, C. Anastasio, Quantum yields of hydroxyl radical and nitrogen dioxide from the photolysis of nitrate on ice. *J. Phys. Chem. A* **107**, 9594–9602 (2003).
26. C. S. Blaszczak-Boxe, A. Saiz-Lopez, Nitrate photolysis in ice and snow: A critical review of its multiphase chemistry. *Atmos. Environ.* **193**, 224–241 (2018).
27. T. Hullar, T. Tran, C. Anastasio, Nitrate photolysis at the air–ice interface of nature-identical snow. *ACS Earth Space Chem.* **7**, 1791–1797 (2023).
28. J. L. France, M. D. King, J. Lee-Taylor, Hydroxyl (OH) radical production rates in snowpacks from photolysis of hydrogen peroxide (H_2O_2) and nitrate (NO_3^-). *Atmos. Environ.* **41**, 5502–5509 (2007).
29. L. Chu, C. Anastasio, Formation of hydroxyl radical from the photolysis of frozen hydrogen peroxide. *J. Phys. Chem. A* **109**, 6264–6271 (2005).
30. U.S. Environmental Protection Agency, Health Risk Assessment/Characterization of the Drinking Water Disinfection Byproduct Bromate (1998).
31. World Health Organization: Geneva, Bromate in Drinking Water (2003).
32. V. I. Furdui, F. Tomassini, Trends and sources of perchlorate in arctic snow. *Environ. Sci. Technol.* **44**, 588–592 (2010).
33. S. Jiang, T. S. Cox, J. Cole-Dai, K. M. Peterson, G. Shi, Trends of perchlorate in Antarctic snow: Implications for atmospheric production and preservation in snow. *Geophys. Res. Lett.* **43**, 9913–9919 (2016).
34. Y. J. Tham, N. Sarnela, S. Iyer, Q. Li, H. Angot, L. L. J. Quéléver, I. Beck, T. Laurila, L. J. Beck, M. Boyer, J. Carmona-García, A. Borrego-Sánchez, D. Roca-Sanjuán, O. Peräkylä, R. C. Thakur, X.-C. He, Q. Zha, D. Howard, B. Blomquist, S. D. Archer, L. Bariteau, K. Posman, J. Hueber, D. Helmig, H.-W. Jacobi, H. Junninen, M. Kulmala, A. S. Mahajan, A. Massling, H. Skov, M. Sipilä, J. S. Francisco, J. Schmale, T. Jokinen, A. Saiz-Lopez, Widespread detection of chlorine oxyacids in the Arctic atmosphere. *Nat. Commun.* **14**, 1769 (2023).
35. I. Gladich, J. S. Francisco, R. J. Buszek, M. Vazdar, M. A. Carignano, P. B. Shepson, *Ab initio* study of the reaction of ozone with bromide ion. *J. Phys. Chem. A* **119**, 4482–4488 (2015).
36. Q. Liu, L. M. Schurter, C. E. Muller, S. Aloisio, J. S. Francisco, D. W. Margerum, Kinetics and mechanisms of aqueous ozone reactions with bromide, sulfite, hydrogen sulfite, iodide, and nitrite ions. *Inorg. Chem.* **40**, 4436–4442 (2001).
37. L. Artiglia, J. Edebeli, F. Orlando, S. Chen, M.-T. Lee, P. Corral Arroyo, A. Gilgen, T. Bartels-Rausch, A. Kleibert, M. Vazdar, M. Andres Carignano, J. S. Francisco, P. B. Shepson, I. Gladich, M. Ammann, A surface-stabilized ozonide triggers bromide oxidation at the aqueous solution-vapour interface. *Nat. Commun.* **8**, 700 (2017).
38. S. N. Wren, D. J. Donaldson, J. P. D. Abbatt, Photochemical chlorine and bromine activation from artificial saline snow. *Atmos. Chem. Phys.* **13**, 9789–9800 (2013).
39. C. S. Boxe, A. Saiz-Lopez, Multiphase modeling of nitrate photochemistry in the quasi-liquid layer (QLL): Implications for NO_x release from the Arctic and coastal Antarctic snowpack. *Atmos. Chem. Phys.* **8**, 4855–4864 (2008).
40. M. Feltracco, E. Barbaro, G. Formenton, G. Mazzi, S. Striuli, C. Bragato, R. Piazza, C. Barbante, A. Gambaro, The disinfection by-products are in the air: Aerosol measurements in the urban area of Venice. *Atmos. Environ.* **318**, 120224 (2024).
41. S. Frassati, E. Barbaro, C. Rossetti, G. Cozzi, C. Turetta, F. Scoto, M. Roman, M. Feltracco, K. Kim, C. Barbante, A. Gambaro, A. Spolaor, Inorganic iodine and bromine speciation in Arctic snow at picogram-per-grams levels by IC-ICP-MS. *J. Anal. Sci. Technol.* **15**, 49 (2024).
42. E. Barbaro, E. Morabito, E. Gregoris, M. Feltracco, J. Gabrieli, M. Vardè, W. R. L. Cairns, F. Dallo, F. De Blasi, R. Zangrando, C. Barbante, A. Gambaro, Col margherita observatory: A background site in the Eastern Italian Alps for investigating the chemical composition of atmospheric aerosols. *Atmos. Environ.* **221**, 117071 (2020).
43. E. Barbaro, M. Feltracco, D. Cesari, S. Padoan, R. Zangrando, D. Contini, C. Barbante, A. Gambaro, Characterization of the water soluble fraction in ultrafine, fine, and coarse atmospheric aerosol. *Sci. Total Environ.* **658**, 1423–1439 (2019).
44. I. M. Solbrekke, A. Sorteberg, H. Haakenstad, The 3 km Norwegian reanalysis (NORA3)—A validation of offshore wind resources in the North Sea and the Norwegian Sea. *Wind Energ. Sci.* **6**, 1501–1519 (2021).
45. M. Mazzola, A. P. Viola, C. Lanconelli, V. Vitale, Atmospheric observations at the Amundsen-nobile climate change tower in Ny-Ålesund, Svalbard. *Rend. Fis. Acc. Lincei* **27**, 7–18 (2016).
46. F. Neese, Software update: The ORCA program system—Version 5.0. *WIREs Comput. Mol. Sci.* **12**, e1606 (2022).
47. F. Neese, The ORCA program system. *WIREs Comput. Mol. Sci.* **2**, 73–78 (2012).
48. J.-D. Chai, M. Head-Gordon, Long-range corrected hybrid density functionals with damped atom–atom dispersion corrections. *Phys. Chem. Chem. Phys.* **10**, 6615 (2008).
49. S. Grimme, J. Antony, S. Ehrlich, H. Krieg, A consistent and accurate *ab initio* parametrization of density functional dispersion correction (DFT-D) for the 94 elements H-Pu. *J. Chem. Phys.* **132**, 154104 (2010).
50. F. Weigend, R. Ahlrichs, Balanced basis sets of split valence, triple zeta valence and quadruple zeta valence quality for H to Rn: Design and assessment of accuracy. *Phys. Chem. Chem. Phys.* **7**, 3297–3305 (2005).
51. V. Barone, M. Cossi, Quantum calculation of molecular energies and energy gradients in solution by a conductor solvent model. *J. Phys. Chem. A* **102**, 1995–2001 (1998).
52. M. Cossi, N. Rega, G. Scalmani, V. Barone, Energies, structures, and electronic properties of molecules in solution with the C-PCM solvation model. *J. Comput. Chem.* **24**, 669–681 (2003).
53. W. Van Pelt, V. Pohjola, R. Pettersson, S. Marchenko, J. Kohler, B. Luks, J. O. Hagen, T. V. Schuler, T. Dunse, B. Noël, C. Reijmer, A long-term dataset of climatic mass balance, snow conditions, and runoff in Svalbard (1957–2018). *Cryosphere* **13**, 2259–2280 (2019).

Downloaded from https://www.science.org at Uppsala University on May 06, 2026

54. L. Van Kampenhout, J. T. M. Lenaerts, W. H. Lipscomb, W. J. Sacks, D. M. Lawrence, A. G. Slater, M. R. Van Den Broeke, Improving the representation of polar snow and firn in the community Earth system model. *J. Adv. Model Earth Syst.* **9**, 2583–2600 (2017).
55. F. Scoto, G. Pappaccogli, M. Mazzola, A. Donateo, R. Salzano, M. Monzali, F. De Blasi, C. Larose, J.-C. Gallet, S. Decesari, A. Spolaor, Automated observation of physical snowpack properties in Ny-Ålesund. *Front. Earth Sci.* **11**, 1123981 (2023).
56. A. Spolaor, C. Varin, X. Pedeli, J. M. Christille, T. Kirchgeorg, F. Giardi, D. Cappelletti, C. Turetta, W. R. L. Cairns, A. Gambaro, A. Bernagozzi, J. C. Gallet, M. P. Björkman, E. Barbaro, Source, timing and dynamics of ionic species mobility in the Svalbard annual snowpack. *Sci. Total Environ.* **751**, 141640 (2021).
57. E. Barbaro, C. Varin, X. Pedeli, J. M. Christille, T. Kirchgeorg, F. Giardi, D. Cappelletti, C. Turetta, A. Gambaro, A. Bernagozzi, J. C. Gallet, M. P. Björkman, A. Spolaor, Dynamics of ionic species in Svalbard annual snow: The effects of rain event and melting. [Preprint] (2019); https://doi.org/10.5194/tc-2019-124.
58. D. G. Liakos, M. Sparta, M. K. Kesharwani, J. M. L. Martin, F. Neese, Exploring the accuracy limits of local pair natural orbital coupled-cluster theory. *J. Chem. Theory Comput.* **11**, 1525–1539 (2015).
59. C. Riplinger, F. Neese, An efficient and near linear scaling pair natural orbital based local coupled cluster method. *J. Chem. Phys.* **138**, 034106 (2013).
60. C. Riplinger, P. Pinski, U. Becker, E. F. Valeev, F. Neese, Sparse maps—A systematic infrastructure for reduced-scaling electronic structure methods. II. Linear scaling domain based pair natural orbital coupled cluster theory. *J. Chem. Phys.* **144**, 024109 (2016).
61. Y. Zhao, D. G. Truhlar, The M06 suite of density functionals for main group thermochemistry, thermochemical kinetics, noncovalent interactions, excited states, and transition elements: Two new functionals and systematic testing of four M06-class functionals and 12 other functionals. *Theor. Chem. Account* **120**, 215–241 (2008).
62. C. Lee, W. Yang, R. G. Parr, Development of the Colle-Salvetti correlation-energy formula into a functional of the electron density. *Phys. Rev. B* **37**, 785–789 (1988).
63. A. D. Becke, A new mixing of Hartree–Fock and local density-functional theories. *J. Chem. Phys.* **98**, 1372–1377 (1993).
64. S. H. Vosko, L. Wilk, M. Nusair, Accurate spin-dependent electron liquid correlation energies for local spin density calculations: A critical analysis. *Can. J. Phys.* **58**, 1200–1211 (1980).
65. P. J. Stephens, F. J. Devlin, C. F. Chabalowski, M. J. Frisch, Ab initio calculation of vibrational absorption and circular dichroism spectra using density functional force fields. *J. Phys. Chem.* **98**, 11623–11627 (1994).
66. G. Henkelman, H. Jónsson, Improved tangent estimate in the nudged elastic band method for finding minimum energy paths and saddle points. *J. Chem. Phys.* **113**, 9978–9985 (2000).
67. D. Trogolo, J. S. Arey, P. R. Tentscher, Gas-phase ozone reactions with a structurally diverse set of molecules: Barrier heights and reaction energies evaluated by coupled cluster and density functional theory calculations. *J. Phys. Chem. A* **123**, 517–536 (2019).
68. S. Brydon, P. Szabó, P. Wongsomboon, B. Poad, D. Marshall, B. Miljevic, A. Trevitt, E. Bieske, J. Harvey, S. Blanksby, Halving the barrier to gas-phase oxidation of bromide by ozone. [Preprint] (2025); https://doi.org/10.26434/chemrxiv-2025-z2rqs.
69. A. Fischbacher, K. Löppenberg, C. Von Sonntag, T. C. Schmidt, A new reaction pathway for bromite to bromate in the ozonation of bromide. *Environ. Sci. Technol.* **49**, 11714–11720 (2015).
70. T. Ingham, D. Bauer, J. Landgraf, J. N. Crowley, Ultraviolet–visible absorption cross sections of gaseous HOBr. *J. Phys. Chem. A* **102**, 3293–3298 (1998).
71. J. B. Burkholder, S. P. Sander, J. Abbatt, J. R. Barker, R. E. Huie, C. E. Kolb, M. J. Kurylo, V. L. Orkin, D. M. Wilmouth, P. H. Wine, Chemical Kinetics and Photochemical Data for Use in Atmospheric Studies: Evaluation No. 19. (JPL Publication 19-5, 2020).

Acknowledgments: We would like to thank all our colleagues at the CNR Dirigibile Italia Arctic Station for support and contributions during the field campaign. This work is the result of multidisciplinary and interdisciplinary research activities conducted at the Arctic Station Dirigibile, which is managed and coordinated by the Institute of Polar Sciences of the National Research Council of Italy. We also thank Elga Lab Water, High Wycombe, UK for supplying the pure water systems used in this study. **Funding:** This research was supported by the Programma di Ricerca in Artico (PRA; project no. PRA2019-0011, Sentinel) and funded by the Italian Ministry of University and Research (MIUR) within the framework of the project "Rain-On-Snow (RoS) Events: How Their Composition Influences Snow Properties in the High Arctic (ROSETTA)" (PRIN 2022LSC4BR). In addition, this study was funded by the Italian Ministry of University and Research (MIUR) as part of the Arctic Research Program of Italy under the project "BETHA-NyÅ—Boundary Layer Evolution Through Harmonization of Aerosol Measurements at Ny-Ålesund Research Station" (PRA2021-0020). We also extend our gratitude to the BioProxies Arctic Field Grant (RiS ID: 12103) project for providing the GSRS daily snow samples. This work was supported by the Korea Polar Research Institute (KOPRI) grant funded by the Ministry of Oceans and Fisheries (KOPRI PE25120). **Author contributions:** Conceptualization: S.F., E.B., F.D.A., A.G., C.B., and A.S. Methodology: S.F., E.B., K.K., A.S.-L., J.S.F., F.W., D.C., A.G., C.B., and A.S. Validation: S.F., E.B., A.G., and A.S. Investigation: S.F., E.B., C.T., G.C., C.R., M.R., A.S.-L., D.C., S.L., and A.S. Formal analysis: C.T., C.R., M.F., and A.S. Data curation: S.F., C.T., and A.S. Software: W.V.P., S.L., and G.B. Resources: F.S., F.B., A.G., C.B., and A.S. Visualization: S.F. and A.S. Supervision: F.D.A., C.B., and A.S. Funding acquisition: E.B., K.K., F.B., C.B., A.G., and A.S. Project administration: C.B. and A.S. Writing—original draft: S.F., E.B., J.S.F., D.C., F.D.A., and A.S. Writing—review and editing: S.F., E.B., F.S., C.R., M.R., K.K., F.B., A.S.-L., J.S.F., W.V.P., F.W., D.C., S.L., G.B., F.D.A., C.B., A.G., and A.S. **Competing interests:** The authors declare that they have no competing interests. **Data, code, and materials availability:** All data and code needed to evaluate and reproduce the results in the paper are present in the paper and/or the Supplementary Materials. There are no new materials generated in the study.

Submitted 10 July 2025
Accepted 12 March 2026
Published 17 April 2026
10.1126/sciadv.aea3286

Downloaded from https://www.science.org at Uppsala University on May 06, 2026

ScienceAdvances

Seasonal bromate formation in the Arctic snowpack: Implications for the bromine biogeochemical cycle

Stefano Frassati, Elena Barbaro, Giulio Cozzi, Clara Turetta, Federico Scoto, Claudia Rossetti, Marco Roman, Matteo Feltracco, Kitae Kim, François Burgay, Alfonso Saiz-Lopez, Joseph S. Francisco, Ward Van Pelt, Feiyue Wang, David Cappelletti, Sofia Lerda, Giovanni Bistoni, Filippo De Angelis, Carlo Barbante, Andrea Gambaro, and Andrea Spolaor

Sci. Adv. **12** (16), eaea3286. DOI: 10.1126/sciadv.aea3286

View the article online
https://www.science.org/doi/10.1126/sciadv.aea3286
Permissions
https://www.science.org/help/reprints-and-permissions

Downloaded from https://www.science.org at Uppsala University on May 06, 2026

Use of this article is subject to the Terms of service

Science Advances (ISSN 2375-2548) is published by the American Association for the Advancement of Science. 1200 New York Avenue NW, Washington, DC 20005. The title *Science Advances* is a registered trademark of AAAS.

Copyright © 2026 The Authors, some rights reserved; exclusive licensee American Association for the Advancement of Science. No claim to original U.S. Government Works. Distributed under a Creative Commons Attribution NonCommercial License 4.0 (CC BY-NC).